www.czasopisma.pan.pl PAN www.journals.pan.pl

ARCHIVES of FOUNDRY ENGINEERING

ISSN (2299-2944)
Volume 19
Issue 1/2019

75 – 82

DOI: 10.24425/afe.2018.125195

13/1

Published quarterly as the organ of the Foundry Commission of the Polish Academy of Sciences

Characterization of $Ca_{50}Mg_{20}Zn_{12}Cu_{18}$ Alloy

B. Hrapkowicz *, S.T. Lesz
Silesian University of Technology, Institute of Engineering Materials and Biomaterials
18A Konarskiego Str. 44-100 Gliwice, Poland
* Corresponding author. e-mail: bartlomiej.hrapkowicz@polsl.pl

Received 10.01.2019; accepted in revised form 10.02.2019

Abstract

The $Ca_{50}Mg_{20}Zn_{12}Cu_{18}$ was assessed with different methods in order to characterize its basic characteristics, and to determine whether the amorphous alloy of such composition would be applicable as an implant material. The XRD analysis was conducted to conclude the structure of the initial material. The $Ca_{50}Mg_{20}Zn_{12}Cu_{18}$ ingot sample demonstrates crystalline structure containing two main intermetallic phases, however as-cast plates show features of an amorphous material, revealing the characteristic amorphous halo on the x-ray patterns. It was confirmed by the scanning electron microscopy method and fracture images revealing chevron pattern morphology with shell type fracture. Corrosion resistance, was studied using the potentiostatic analysis. The amorphous samples show higher resistance than the crystalline one. Post corrosion surface of the $Ca_{50}Mg_{20}Zn_{12}Cu_{18}$ alloy exhibits high concentration of magnesium and calcium hydroxides, forming the globular structures in large aggregates of spherical units.

Keywords: Calcium alloy, Implant; metallic glass, Magnesium, Calcium, Zinc, Copper, Corrosion, Corrosion resistance

1. Introduction

Various metal alloys are becoming more and more important in modern implantology, together with ceramics and polymers that are used as biomaterials to perform specific functions or act as complementary organs or tissues. These materials must be characterized by certain specific features, with biocompatibility and lack of toxicity at the forefront. In addition, their durability and general resistance to the aggressive environment (which is the interior of the human body) is also crucial [1]. Due to the requirements of titanium or stainless steel for biomaterials, they are irreplaceable, but their price and osseointegration still need to be refined. The research is also conducted with different classes of materials, among which there is bioactive glass or ceramics such as hydroxyapatite and apatite-wollastonite. Ceramics are highly biocompatible, because they contain natural ions for the body, such as Ca2+, K+, Na+ etc. which cause specific behavior between the implant and the body. Their disadvantage, however, is the lack of adequate strength, which makes them suitable only for small fillings such as ones used in dentistry [1].

The solution to this problem may be amorphous materials due to their metal-like strength properties, lightness and better corrosive properties than some of the crystalline alloys used. In his work, Zberg carried out in vivo studies using MgZnCa metallic glasses, which showed biocompatibility and lower hydrogen evolution [2]; [3]. Due to the combination of biocompatibility and mechanical properties, metallic glasses seem to be a good way to develop implantology [4]; [5].

During the selection of various components for the material of the eventual implant, various materials are taken into consideration. The most important point was to prepare the implant to employ a biodegradable role. This means that all of the materials would have to possess some characteristics making them beneficial for the body during mending period. The definition of biodegradability is the process of degradation of the material upon contact with the environment of an organism. Usually it means to be broken down by microorganisms [6]. Bones are mostly composed of calcium, that is why this element is used for the implant. Calcium is abundant in the human organism. It is crucial for the bones and teeth as it ensures their durability. Moreover ionized calcium fulfils very important

biological task influencing the blood coagulation process, the permeability of cell membranes, regulates the excitability of both the nervous and muscle system. This is vital because calcium contained in the implant will not affect the body in any way until it begins to break down, because it won't be ionized before that. Moreover calcium controls the magnesium concentration, lowering it if necessary, hence preventing hypermagnesemia. As the mechanical properties are considered Ca and Mg alloys affect each other, where Ca improve corrosion resistance and grain refinement [7].

On the other hand magnesium is a natural Ca antagonist, meaning that it controls the calcium concentration and vice versa. Magnesium is vital for human body as it controls the enzyme activation.

The two aforementioned materials are crucial for this kind of implant. That being said they alone may not possess adequate strength properties to employ such a function as the stresses and the wear of an implant are quite significant, which obviously is the case for crystalline materials. Moreover amorphous materials are known to possess better mechanical and corrosion resistance than their crystalline counterparts [8]; [9]. Thus it is only proper to add another alloying elements which would improve the quality and strength of such a device. One of such elements can be zinc. Mechanically speaking Zn improves yield stress and reduce hydrogen gas evolution during biocorrosion [7]. This is specifically important as hydrogen creates gas cavities [2]; [10]. Normally they are dealt with by simple puncture of the cavity, hence releasing the accumulated gas. Although this solution seem really simple, it may not be applicable in case of certain internal surgeries.

Usually when such a cavity forms, but its size is still small, it poses no problem for the organism because the gas is quickly exchanged with the surrounding tissues. The issue arises when the tissues do not extract the gas quickly enough resulting in large cavity formation, such situations are detrimental as the excessive gas creates pressure inducing various problems such as mechanical disturbances of bone regeneration. There are different methods for tackling that problem, although one of the simplest ones seem to manipulate to the benefit of the alloy composition in order to reduce the hydrogen evolution [11].

The problem with material selection for implants is that they need to ensure its biocompability in order to avoid unnecessary damage for the organism. In case of the biodegradable implants it is sure that the material will corrode and degrade, since it is its goal. Thus it is crucial that the corrosion products should not be toxic. Moreover they should be easily absorbed and dissolved [12]. It was already mentioned that Ca, Mg and Zn may be used as microelements for the body during the healing process, yet there are various problems which have to be considered during an implantation. Despite all of the precautions taken to ensure the aseptic conditions the infections associated with the implantations remain as the most severe complications [13]. Usually they are caused by microorganisms creating a biofilm on the implant enabling the bacteria to resist the immune responses and antibiotics [14]; [15]. However there are several metal ions which possess antibacterial properties. One of such materials is copper. Of course Cu may be considered detrimental to the organisms as there are reports of its negative influence [16], yet it is an essential trace mineral which plays important role in bone growth and maintenance. Its deficiency may cause structural abnormalities of the skeleton such as for example osteoporosis [17]; [18]; [19]. That being said Cu may be a valid material for an implant as it ensures proper Cu amount and employs even more important work which is the anti-inflammatory function blocking the microorganisms from creating the biofilm near the implant. Usually Ag was considered to be an antibacterial material although Cu is characterized by its lower toxicity and higher cytocompability, yet it is not the most important reason. Copper is easily metabolized, meaning that it won't increase copper serum level as opposed to silver [13]; [20]. In this research it is crucial to establish whether amorphous $Ca_{50}Mg_{20}Zn_{12}Cu_{18}$ alloys are superior to crystalline ones. Henceforth their structure, fracture morphologies after mechanical failure and corrosion resistance will be studied, as well as the chemical composition before and after corrosion tests.

2. Experimental procedure

The master alloy with a nominal composition of $Ca_{50}Mg_{20}Zn_{12}Cu_{18}$ in atomic percent was used. Alloy ingot was produced by induction melting mixtures of pure elements (Ca 99.5%, Mg 99.8%, Zn 99.995%, Cu 99.95%) and Mg69Ca31 alloy under an argon atmosphere [4]; [5]; [21]. Then the pieces of the ingot (W1 sample) were remelted several times to ensure chemical homogeneity [3]; [5]. Samples in form of plates with a length and width of 10 mm and a thickness of 1 and 2 mm were prepared by a copper mold casting method.

Obtained representative samples are described in Table 1.

Table 1.
$Ca_{50}Mg_{20}Zn_{12}Cu_{18}$ alloy representative samples

No.	Sample	Comment
1.	W1	Ingot sample
2.	P1	1 mm thick cast plate
3.	P2	2 mm thick cast plate

The structure of the samples (both ingot and plates) was checked by X-Ray diffraction (XRD) method using XRD 7 Seifert-FPM and XRD X'PERT Pro PANalyical diffractometers. The Co Kα radiation source with 0.17902 nm wavelength was used. The diffraction patterns were recorded by "step-scanning" method in the range from 20 to 100 2Θ angle.

The aim of the analysis was to survey the corrosion resistance in the aggressive environment simulating human organism. The samples were polished and washed with 96% ethyl alcohol as according to PN-EN ISO 17475:2010 and PN-EN ISO 11463:2010 standards.

The potentiostatic measurements were conducted in Autolab 302N workstation at the temperature of 37°C. Three electrode cell configuration was applied for the electrochemical measurements: a saturated calomel electrode (SCE) as a reference electrode, platinum rod as a counter electrode and sample as the working electrode. The samples were immersed in a Ringer solution (Baxter company). The samples were immersed for a 60 s in order to determine proper potential, and then for 900 s. The scanning speed for the samples was 1 mV/s.

The morphology of fracture surfaces of the samples after decohesion was examined by means of a scanning electron microscope (SEM) SUPRA 35, ZEISS firm, with voltage of 25 kV. Analysis of the chemical composition of the samples on selected areas (microarea or entire micrograph area) before and after corrosion test was performed using an energy-dispersive X-ray spectroscope (EDS, Edax Trident XM4 detector), coupled with the SEM. The EDS analysis was performed to assess the chemical composition of the samples.

3. Results and Discussion

X-Ray diffraction (XRD) patterns in Figure 1 and Figure 2 verify the structures of representative samples.

The research shows that the $Ca_{50}Mg_{20}Zn_{12}Cu_{18}$ alloy has the following characteristics:

All of the samples were examined with SEM equipped with an Energy-dispersive X-ray spectroscopy analyzer. It was done in order to determine whether the ingot and the cast-plates had desired chemical composition. The results are shown in the Table 2, selected samples are further represented (Fig. 3, Fig. 4, Fig. 5).

Table 2.
Chemical composition of the $Ca_{50}Mg_{20}Zn_{12}Cu_{18}$ alloy ingot and plates by EDS analysis

Sample	Chemical composition, At%					
	Ca	Mg	Zn	Cu	Others	Figure
Desired alloy	50	20	12	18	-	-
W1	46.19	26.84	10.94	16.03	-	Fig. 5
	53.07	23.32	11.48	12.12	-	-
	45.84	26.15	12.01	16.00	-	-
Avg.	48.36	25.43	11.47	14.71		
P1	50.89	18.64	12.48	17.98	-	-
	52.51	13.05	14.27	20.18	-	Fig. 3
	52.15	14.24	13.53	20.08	-	-
Avg.	51.85	15.31	13.43	19.41		
P2	50.47	12.48	13.72	19.40	3.92	Fig. 4
	46.70	16.86	10.93	16.32	9.18	-
Avg.	48.59	14.67	12.33	17.86		

The desired chemical composition of the alloy was as the name suggests $Ca_{50}Mg_{20}Zn_{12}Cu_{18}$. It can be seen that the results slightly vary, but they are well in the expected range, the magnesium content in the P1 and P2 samples may be lower due to the evaporation during the casting process. Thanks to this analysis it has been confirmed that the obtained samples had the chemical composition that was expected. As the next step, the samples were examined with a X-ray spectroscopy analysis in order to determine the non- or crystallinity of the ingot and plates.

The $Ca_{50}Mg_{20}Zn_{12}Cu_{18}$ base alloy ingot is crystalline as evidenced by X-ray examinations. X-ray phase analysis results revealed the presence of crystalline phases such as Ca(Cu0.60, Zn0.40) and CaMg2 in the structure of the alloy (Fig. 1).

Examinations of the $Ca_{50}Mg_{20}Zn_{12}Cu_{18}$ alloy in the form of cast plates with a thickness of 1 and 2 mm shows a broad peak corresponding to the amorphous phase. The diffuse diffraction halos are characteristic for the amorphous state but are not sufficient do describe the atomic arrangements within the solid (Fig. 2).

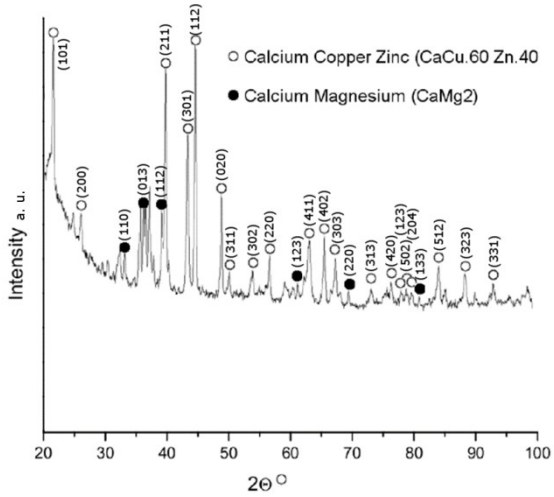

Fig. 1. XRD pattern of the $Ca_{50}Mg_{20}Zn_{12}Cu_{18}$ alloy ingot

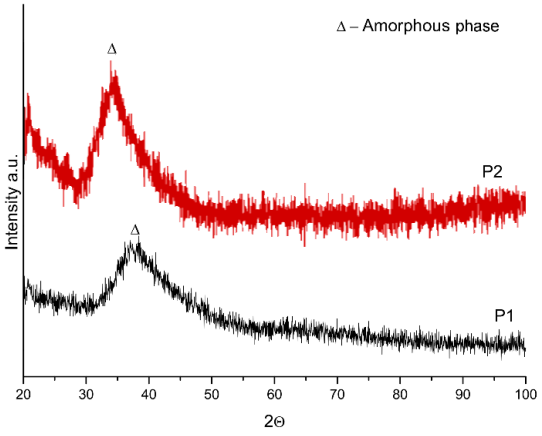

Fig. 2. XRD pattern of selected cast samples of the $Ca_{50}Mg_{20}Zn_{12}Cu_{18}$ alloy (P2 on the top and P1 on the bottom)

SEM investigations of the failure surface of the examined alloy ingot had intercrystalline character (Fig. 5). SEM investigations of the fracture of the $Ca_{50}Mg_{20}Zn_{18}Cu_{12}$ alloy plates with 1 mm (Fig. 3) and 2 mm thickness (Fig. 4) showed typical morphology of the amorphous alloys. Fracture surface showed chevron pattern morphology with shell type fracture (Fig. 3, Fig. 4) [4]; [5]; [22]. A similar surface morphology is shown for $Mg_{65}Li_2Cu_{18}Ni_5Y_{10}$ alloy [23], for $Ca_{50}Mg_{20}Cu_{30}$ and $Mg_{65}Cu_{25}Y_{10}$ alloy [3]; [4]; [5].

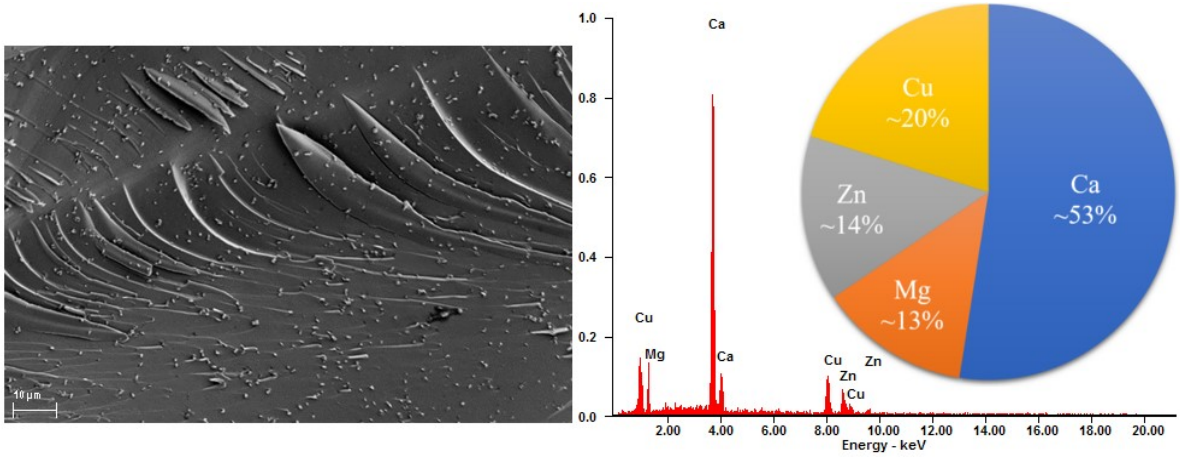

Fig. 3. Fracture morphology of $Ca_{50}Mg_{20}Zn_{12}Cu_{18}$ alloy cast P1 plate with the chemical composition on the EDS graph and graphical representation of the at% composition. EDS spectrum from entire area of the micrograph

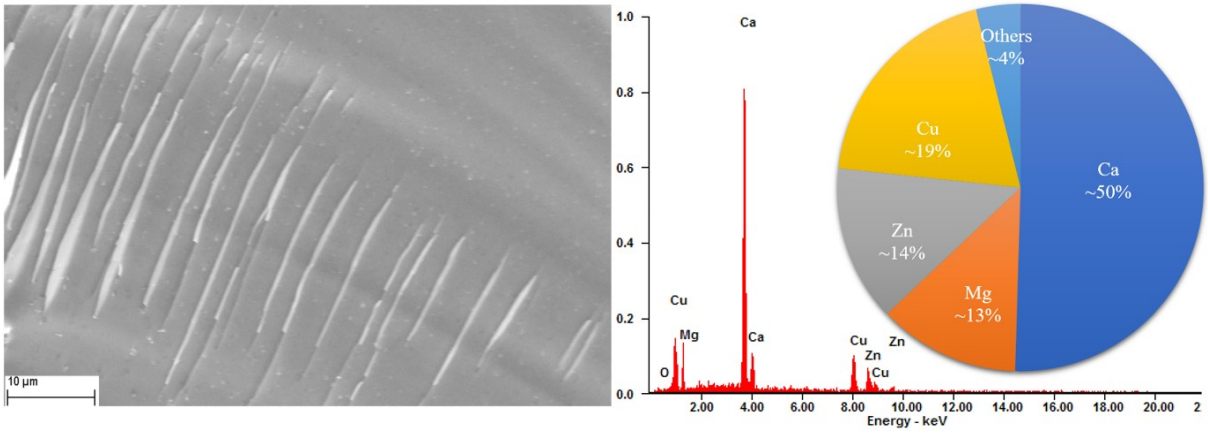

Fig. 4. Fracture morphology of $Ca_{50}Mg_{20}Zn_{12}Cu_{18}$ alloy cast P2 plate with the chemical composition on the EDS graph and graphical representation of the at% composition. EDS spectrum from entire area of the micrograph

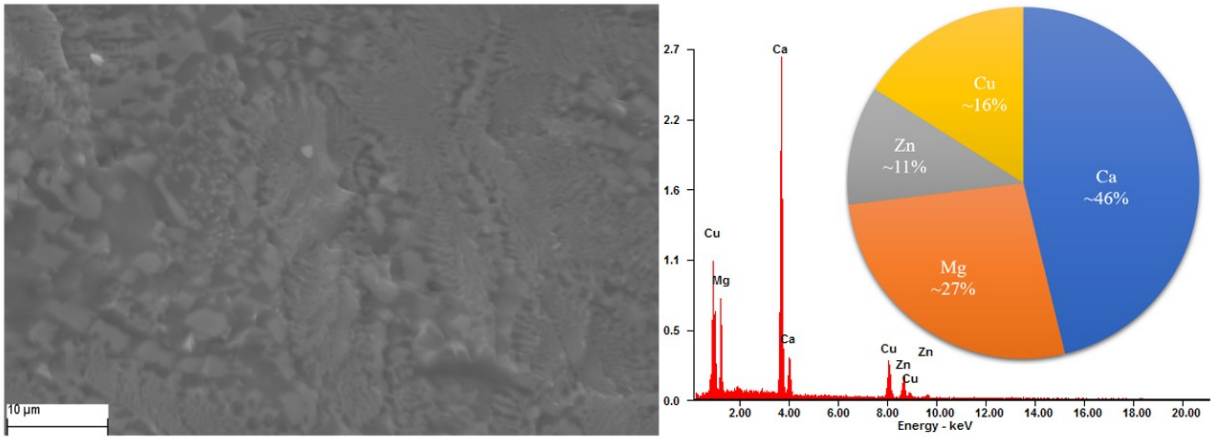

Fig. 5. Fracture morphology of $Ca_{50}Mg_{20}Zn_{12}Cu_{18}$ alloy W1 sample with the chemical composition on the EDS graph and graphical representation of the at% composition. EDS spectrum from entire area of the micrograph

Selected samples were studied with corrosion tests. The potentiostatic studies have shown some characteristic features that prove the formation of the passive layer (Fig. 6 W1).

The results of the potentiostatic analysis of the ingot are clearly different from those obtained for samples in the form of cast plates (Fig. 6 P1 and P2). The potentiostatic curve of the ingot sample (W1) indicates the cyclic process of formation and destruction of the passive layer known as oxidation and reduction, as the curve is not uniform and it can be characterized by different valleys and peaks. It suggests very active reaction on the surface of the sample.

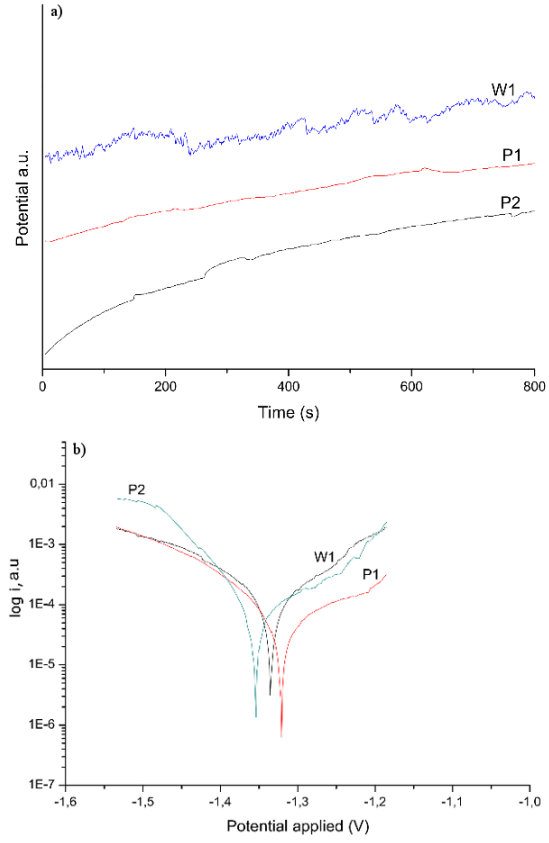

Fig. 6 a) Linear Polarization Resistance curves for the W1, P1 & P2 samples b) Potentiostatic curves for the W1, P1 & P2 samples

Another behavior of the samples during contact with the aggressive Ringer solution environment resulted from their different structure. Corrosion resistance is being represented as corrosion potential E_{corr} and corrosion current density i_{corr}. Moreover as compared to the literature data it can be seen that the values of corrosion density current was similar to the ones presented in the P1 and P2 samples [3]. However, the results of the analysis, allowing the determination of corrosion resistance, deviate from the literature data, which show a higher value of corrosion resistance for that kind of alloys [22]. It can be seen that the samples differed in the corrosion current density, where the ingot sample W1 is characterized by i_{corr} amounting to 6.17 mA/cm^2, as it was to be expected due to its crystalline structure. P1 and P2 are amorphous and can be characterized with corrosion density current which equaled to 2.05 and 3.15 mA/cm^2 respectively, hence better resistance. W1 sample is characterized by uneven curve, which suggests various reactions happening on the sample surface, whereas on both P1 and P2 curves the lines are considerably smoother, although not devoid of any reaction. Interestingly the sample exhibiting better corrosion resistance was the sample of 1 mm width, whereas the 2 mm sample was slightly worse. There are different reasons why the samples may exhibit different behavior. There could be a slight difference in the polishing process or the conditions of the experiment could be a little bit different, moreover the samples might not be fully amorphous. Due to the larger thickness of the P2 sample its structure might have started to order, thus decreasing the corrosion resistance. As it can be seen on the XRD results shown in the Fig. 2 the P1 pattern is smoother as compared to the P2 pattern. However this pattern (Fig. 2 P2) does not confirm the changes in the phase composition of the structure. The results in the Table 3 are backed up by the potentiostatic curves in Fig. 6 b. The results of the potentiostatic study have shown that 1 mm sample is the least active one of all, as the curves are smoothest ones as compared to the other samples, moreover both W1 and P2 samples derive slightly to the left and upper side of the graph, meaning the applied potential was higher, as well as the current density. Those two factors mean that the reactions happening on those samples are more violent and faster, which can be seen as the many peaks and valleys on the curves [24]. The E_{corr} of the samples varied between -1.32 and -1.35 V. Existing data on similar Ca and Mg-based alloys has been reported by Morrison et al. [22] obtaining -1.54 V for $Ca_{65}Mg_{15}Zn_{20}$ in the Na_2SO_4 electrolyte, while Zberg et al. [2] obtained -1.28 V for $Mg_{66}Zn_{29}Ca_5$ in SBF27 without NaN. Due to varying experiment parameters it is difficult to compare actual E_{corr} values [25].

Table 3.
Corrosion current density and potential for selected samples of the $Ca_{50}Mg_{20}Zn_{12}Cu_{18}$ alloy (E_{corr} – Corrosion potential, i_{corr} – corrosion current density

Sample	E_{corr}, V	i_{corr}, mA/cm^2
W1	-1.34	6.17
P1	-1.32	2.05
P2	-1.35	3.15
$Ca_{50}Mg_{20}Cu_{30}$ as-cast *	-1.25	2.12
$Ca_{50}Mg_{20}Cu_{30}$ 573 K/1h*	-1.26	3.11
$Ca_{55}Mg_{18}Zn_{11}Cu_{16}$ **	-0.48	-
$Ca_{50}Mg_{20}Cu_{30}$ **	-1.17	-

*[3] **[22]

After the corrosion tests, the samples exposed to the Ringer solution were analysed using an EDS in order to determine the chemical compositions, which were expected to be drastically changed after the immersion. The results of the analysis are presented in Table 4.

It is worth noting that the chemical composition changed drastically as compared to the results presented in the Table 2. The EDS analysis exhibited the presence of alloying elements as Ca, Mg, Zn, Cu as expected, additionally O, C and Al were present. High O presence may indicate that both oxides and hydroxides could form on the surface of the sample. It is reported

as well by Babilas et al. [24] and Morrison et al. [22]. The carbon and aluminum may be remnants of the polishing process as the polishing papers are made of corundum (Al_2O_3) and silicon carbide (SiC). The W1 sample can be characterized with the highest oxygen count and the sharpest decline of the primary elements, the surface morphology of the W1 sample and the EDS representation are shown in Fig. 7. It can be explained with its crystalline structure which reacts more actively with the corrosive environment.

Table 4.
Chemical composition of the $Ca_{50}Mg_{20}Zn_{12}Cu_{18}$ alloy ingot and plates, post-corrosion test, by EDS analysis

Sample/ Figure	Chemical composition, at%						
	Ca	Mg	Zn	Cu	Others		
					O	C	Al
W1 Fig. 7	29.70	02.92	01.16	01.23	51.79	13.20	-
P1 Fig. 8	42.60	00.98	00.67	00.89	43.82	10.43	00.62
P2 Fig. 9	36.13	10.98	07.80	10.22	14.06	18.62	02.19

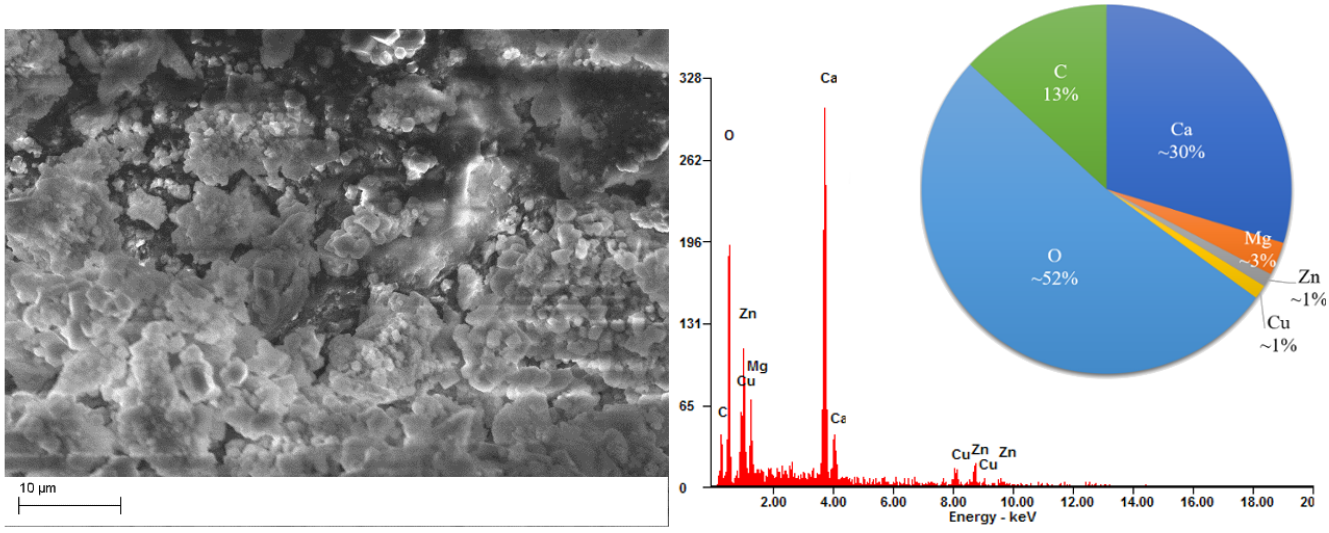

Fig. 7. Surface morphology of the $Ca_{50}Mg_{20}Zn_{12}Cu_{18}$ alloy W1 sample after potentiostatic tests with X-ray analysis (EDS) representation observed after potentiostatic tests for the W1 sample of the $Ca_{50}Mg_{20}Zn_{12}Cu_{18}$ alloy with graphic at% chemical composition representation. EDS spectrum from entire area of the micrograph

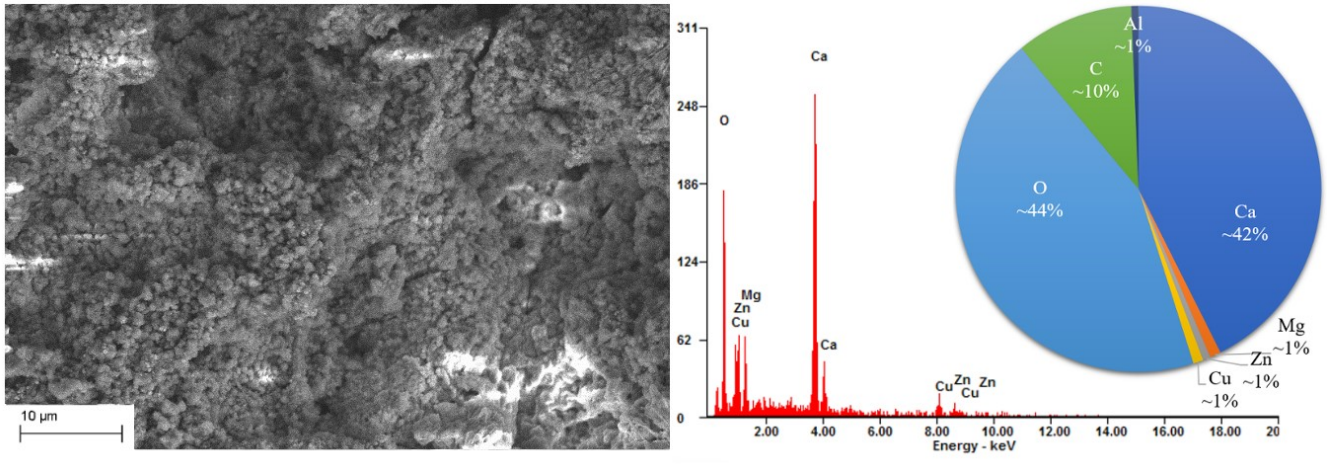

Fig. 8. Surface morphology of the $Ca_{50}Mg_{20}Zn_{12}Cu_{18}$ alloy sample P1 with X-ray analysis (EDS) representation observed after potentiostatic tests for the P1 sample of the $Ca_{50}Mg_{20}Zn_{12}Cu_{18}$ alloy. EDS spectrum from entire area of the micrograph

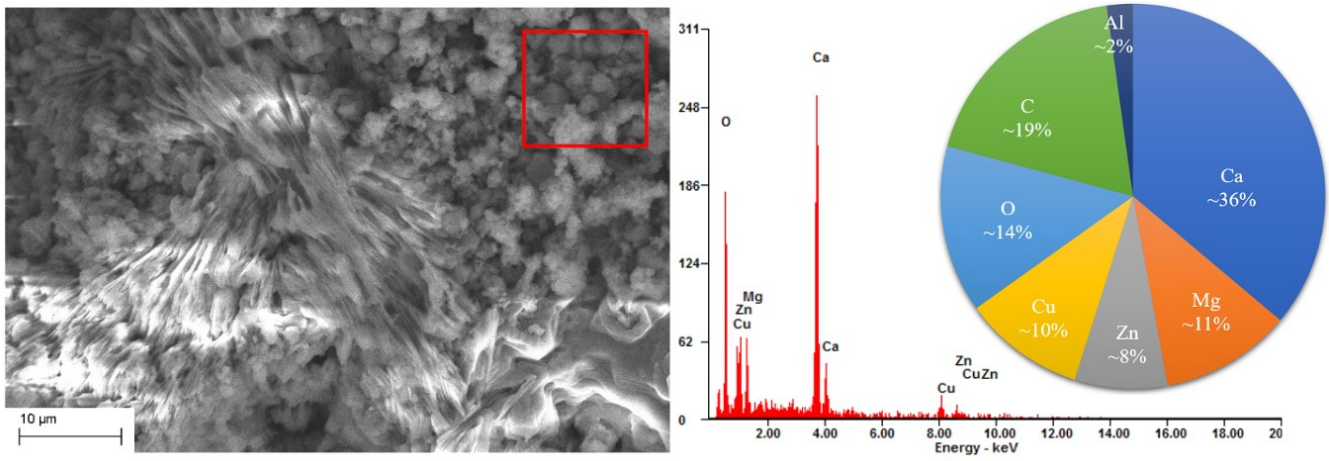

Fig. 9. Surface morphology of the $Ca_{50}Mg_{20}Zn_{12}Cu_{18}$ alloy sample P2 with X-ray analysis (EDS) representation observed after potentiostatic tests for the P2 sample of the $Ca_{50}Mg_{20}Zn_{12}Cu_{18}$ alloy. EDS spectrum from the area marked by the square indicator

The surface morphologies of both P1 and P2 samples are presented in Fig. 8 and Fig. 9 respectively. It can be seen that the surfaces of the samples are not uniform, it is a result of the potentiostatic analysis which caused the corrosion products to appear. As it is reported by Henrist et al. [26] and Rodriguez-Navarro et al. [27] when the concentration of magnesium and calcium hydroxides increases, the globular structures can be observed, moreover large aggregates of spherical units are formed, and they can be seen in both Fig. 8 and Fig. 9. It is proven that the samples did corrode as it was mentioned before, but the EDS results clearly show high oxygen count which equals to the oxides presence.

The literature data affirms the formation of a protective layer [22]. These results confirm that metallic glasses are more resistant to corrosion than crystalline materials (Fig. 6 and Table 3).

4. Conclusions

The initial ingot of the $Ca_{50}Mg_{20}Zn_{12}Cu_{18}$ alloy has a crystalline structure which consisted of two main intermetallic phases: Ca(Cu0,60,Zn0,40) and $CaMg_2$. The plate samples of the same alloy were characterized by the amorphous structure. The fracture morphology of the samples revealed two types of fracture, chevron pattern morphology with shell type fracture. Basing on the potentiostatic analysis it was determined that the $Ca_{50}Mg_{20}Zn_{12}Cu_{18}$ alloy corrosion analysis varied depending on its microstructure, and it was visibly better for the amorphous structure as compared to the crystalline one. Although, it was not high enough to withstand the aggressive environment of the human body and rapid dissolution took place. It was clear due to observed globular structures aggregated in spherical units and EDS results that considerable amount of calcium and magnesium oxides and hydroxides were formed postcorrosion, hence the corrosion morphology observed in the $Ca_{50}Mg_{20}Zn_{12}Cu_{18}$ alloy has been typical for that kind of alloy.

Acknowledgments

This work was financially supported with statutory funds of Faculty of Mechanical Engineering of Silesian University of Technology in 2018.

References

[1] Mihov, D. & Katerska, B. (2010). Some biocompatible materials used in medical practice. *Trakia Journal of Sciences*. 8(8), 119-125. https://doi.org/10.2320/matertrans.L-MRA2008828.

[2] Zberg, B., Uggowitzer, P.J. & Löffler, J.F. (2009). MgZnCa glasses without clinically observable hydrogen evolution for biodegradable implants. *Nature Materials*. 8, 887. http://dx.doi.org/10.1038/nmat2542.

[3] Babilas, R., Cesarz-Andraczke, K., Babilas, D. & Simka, W. (2015). Structure and Corrosion Resistance of Ca50Mg20Cu30 Bulk Metallic Glasses. *Journal of Materials Engineering and Performance*. 24(1), 167-174. https://doi.org/10.1007/s11665-014-1308-x.

[4] Senkov, O.N., Scott, J.M. & Miracle, D.B. (2008). Effect of Al addition on glass forming ability and glass stability of Ca-Mg-Zn-Cu based bulk metallic glasses. *Metallurgical and Materials Transactions A: Physical Metallurgy and Materials Science*. 39(8), 1901-1907. https://doi.org/10.1007/s11661-007-9255-x.

[5] Nowosielski, R., Babilas, R., Guwer, A. & Borowski, A. (2012). Fabrication of Mg 65 Cu 25 Y 10 bulk metallic glasses. *Archives of Materials Science and Engineering*. 53(2), 77-84.

[6] Anderson, J.M. (1983f). Biological performance of materials-fundamentals of biocompatibility (Vol. 8, Biomedical engineering and instrumentation series), by Jonathan Black, Marcel Dekker, New York, NY, 1981. *Journal of Biomedical Materials Research*. 17(3), 557-558. https://doi.org/10.1002/jbm.820170313.

[7] Radha, R. & Sreekanth, D. (2017). Insight of magnesium alloys and composites for orthopedic implant applications – a review. *Journal of Magnesium and Alloys*. 5(3), 286-312. https://doi.org/10.1016/J.JMA.2017.08.003.
[8] Byrne, J.H., O'Cearbhaill, E.D. & Browne, D.J. (2015). Comparison of crystalline and amorphous versions of a magnesium-based alloy: corrosion and cell response.
[9] Gilman, J.J. (1975). Mechanical behavior of metallic glasses. *Journal of Applied Physics*. 46(4), 1625-1633. https://doi.org/10.1063/1.321764.
[10] Kuhlmann, J., Bartsch, I., Willbold, E., Schuchardt, S., Holz, O., Hort, N. & Heineman, W.R. (2013). Fast escape of hydrogen from gas cavities around corroding magnesium implants. *Acta Biomaterialia*. 9(10), 8714-8721. https://doi.org/10.1016/J.ACTBIO.2012.10.008.
[11] Noviana, D., Paramitha, D., Ulum, M.F. & Hermawan, H. (2016). The effect of hydrogen gas evolution of magnesium implant on the postimplantation mortality of rats. *Journal of Orthopaedic Translation*. 5, 9-15. https://doi.org/10.1016/J.JOT.2015.08.003.
[12] Eddy Jai Poinern, G., Brundavanam, S. & Fawcett, D. (2013). Biomedical magnesium alloys: a review of material properties, surface modifications and potential as a biodegradable orthopaedic implant. *American Journal of Biomedical Engineering*. 2(6), 218-240. https://doi.org/10.5923/j.ajbe.20120206.02.
[13] Bergemann, C., Zaatreh, S., Wegner, K., Arndt, K., Podbielski, A., Bader, R., … Nebe, J.B. (2017). Copper as an alternative antimicrobial coating for implants - An in vitro study. *World Journal of Transplantation*. 7(3), 193-202. https://doi.org/10.5500/wjt.v7.i3.193.
[14] Costerton, J.W., Stewart, P.S. & Greenberg, E.P. (1999). Bacterial biofilms: a common cause of persistent infections. *Science (New York, N.Y.)*. 284(5418), 1318-1322. Retrieved from http://www.ncbi.nlm.nih.gov/pubmed/10334980.
[15] Davies, D. (2003). Understanding biofilm resistance to antibacterial agents. *Nature Reviews Drug Discovery*. 2(2), 114-122. https://doi.org/10.1038/nrd1008.
[16] Solomons, N.W. (1985). Biochemical, metabolic, and clinical role of copper in human nutrition. *Journal of the American College of Nutrition*. 4(1), 83-105. Retrieved from http://www.ncbi.nlm.nih.gov/pubmed/3921587.
[17] Tümer, Z. & Møller, L.B. (2010). Menkes disease. *European Journal of Human Genetics: EJHG*, 18(5), 511-518. https://doi.org/10.1038/ejhg.2009.187.
[18] Mahdavi-Roshan, M., Ebrahimi, M. & Ebrahimi, A. (2015). Copper, magnesium, zinc and calcium status in osteopenic and osteoporotic post-menopausal women. *Clinical Cases in Mineral and Bone Metabolism: The Official Journal of the Italian Society of Osteoporosis, Mineral Metabolism, and Skeletal Diseases*, 12(1), 18-21. https://doi.org/10.11138/ccmbm/2015.12.1.018.
[19] Pepa, G. Della, & Brandi, M.L. (2016). Microelements for bone boost: the last but not the least. *Clinical Cases in Mineral and Bone Metabolism: The Official Journal of the Italian Society of Osteoporosis, Mineral Metabolism, and Skeletal Diseases*. 13(3), 181-185. https://doi.org/10.11138/ccmbm/2016.13.3.181.
[20] Massè, A., Bruno, A., Bosetti, M., Biasibetti, A., Cannas, M., & Gallinaro, P. (2000). Prevention of pin track infection in external fixation with silver coated pins: clinical and microbiological results. *Journal of Biomedical Materials Research*. 53(5), 600-604. Retrieved from http://www.ncbi.nlm.nih.gov/pubmed/10984710.
[21] Amiya, K., & Inoue, A. (2002). Formation, thermal stability and mechanical properties of ca-based bulk glassy alloys. *MATERIALS TRANSACTIONS*. 43(1), 81-84. https://doi.org/10.2320/matertrans.43.81.
[22] Morrison, M.L., Buchanan, R.A., Liaw, P.K., Senkov, O.N. & Miracle, D.B. (2006). Electrochemical behavior of Ca-based bulk metallic glasses. *Metallurgical and Materials Transactions A*, 37(April), 1239-1245. https://doi.org/10.1007/s11661-006-1075-x.
[23] Liu, G., Gao, P., Xue, Z., Tong, Z., & Zhang, M. (2011). Ultrahigh strength Mg–Li based bulk metallic glasses: Preparation and performance research. *Materials Science and Engineering A-structural Materials Properties Microstructure and Processing - Mater Sci Eng A-Struct Mater*. 528. https://doi.org/10.1016/j.msea.2011. 06.012.
[24] Babilas, R., Bajorek, A., Hawełek, Ł., Głuchowski, W., Simka, W. & Babilas, D. (2017). Structural and electrochemical characterization of the Ca50Mg20Cu25Zn5 amorphous alloy. *Journal of Non-Crystalline Solids*. 471, 467-475. https://doi.org/10.1016/J.JNONCRYSOL.2017.07.006.
[25] Cao, J.D., Kirkland, N.T., Laws, K.J., Birbilis, N. & Ferry, M. (2012). Ca–Mg–Zn bulk metallic glasses as bioresorbable metals. *Acta Biomaterialia*. 8(6), 2375-2383. https://doi.org/10.1016/J.ACTBIO.2012.03.009.
[26] Henrist, C., Mathieu, J.-P., Vogels, C., Rulmont, A. & Cloots, R. (2003). Morphological study of magnesium hydroxide nanoparticles precipitated in dilute aqueous solution. *Journal of Crystal Growth*. 249(1-2), 321-330. https://doi.org/10.1016/S0022-0248(02)02068-7.
[27] Rodriguez-Navarro, C., Hansen, E., & Ginell, W. S. (2005). Calcium hydroxide crystal evolution upon aging of lime putty. *Journal of the American Ceramic Society*. 81(11), 3032-3034. https://doi.org/10.1111/j.1151-2916.1998.tb02735.x.